Indian Journal of Engineering & Materials Sciences
Vol. 31, February 2024, pp. 93-107
DOI: 10.56042/ijems.v31i1.6444

XPS analysis of oxidized Fe based alloy ribbons

N Karar[a]

CSIR-National Physical Laboratory, Dr. KS Krishnan Road, New Delhi, 110 012, India

Received: 28 October 2023; Accepted: 22 January 2024

X-ray photoelectron spectroscopy (XPS) results from a set of experimental grade oxidized, iron based alloys of varying compositions, and oxidization levels and having different crystalline phases and structures are compared and correlated. It is shown how their binding energy profile-contours can vary from alloy to alloy for the same elements which are present in different proportions under varying preparation conditions. Such XPS analysis was more successful for cross-checking composition w.r.t. other analytical techniques like Energy dispersive X-ray analysis (EDAX) or X-ray fluorescence methods (XRF). Changes in crystallinity, composition, sample preparation conditions, oxidation and related phase changes contributed significantly to observed chemical changes in these alloy samples. In non-electronic grade materials, observing unexpected impurities can be common. So, such XPS analysis helps estimate the likely performance of an alloy and also detects the extent of unwanted impurities at the preparation stage itself that may affect the performance.

Keywords: X-ray photoelectron spectroscopy, Iron based alloy ribbons, Oxidization, Impurities

1 Introduction

Metals have been used from infinite time past, since antiquity, possibly for the last several thousand years for its durability, hardness and strength. Metals have aided the progress in civilization up to the limit to which man has been able to be imaginative in its applications in furthering the growth of civilization. Metal alloying is a process in which different metals have been mixed, whether by intent or otherwise, resulting in much better quality of metals which are better suited in terms of their performance, under certain relatively more demanding processes, under more demanding ambient conditions and which are also more durable for a longer time. This has been a cyclic process, with a certain alloy being first invented with certain expectations, and after it gave significant improvements to contemporary usage, further composition optimization was attempted. Such progress of civilization in turn has lead to demands for even more improved alloys in various ferrous and non ferrous categories[1].

With progress in civilization, man has progressively discovered different alloys, their subsequent possible applications and then how to ensure their repeatability during production processes. Man has also discovered X-rays in the last 120 years or so, and then slowly learnt how to use this X-ray directly and indirectly to further analyse different metals and their alloys. This has lead to the development of different independent analytical techniques, like X-ray Diffraction (XRD), X-ray fluorescence (XRF), Energy Dispersive X-Ray (EDAX), and later the X-Ray Photoelectron Spectroscopy (XPS)[2]. XRD has now evolved to distinguish crystalline and amorphous materials and then to understand crystalline periodicity issues. Thus, different metals and alloys are distinguishable in terms of their different XRD patterns alone. Almost all other forms of such X-ray based techniques are about detecting the chemical constituents of different materials. Each of these techniques has its own advantages and disadvantages. XRF and EDAX are capable to give us the approximate elemental composition, but they do not say anything about their possible chemical bonding profile, or to what extent an alloy or constituent element has corroded, or whether two or more elements have just mixed with each other as in a physical mixture or if there has been any chemical bonding among them etc. etc. - as an example, the formation of iron oxide coating on iron and adsorption of oxygen in iron. Chemical bonding formation often leads to much more stronger materials. Metallic bonds in metals and alloys are weak compared to covalent bonds in ceramics. Strengthening in metals and alloys take place due to mechanisms like grain refinement, cold working, precipitation structures etc.

*Corresponding Author (E-mail: nkarar78@gmail.com)

So, a more detailed chemical bond related analysis of different metals and their alloys are required. It can be obtained only from a detailed XPS analysis. XPS also gives quantitative information on alloying content, including on metal constituents, their proportions and their oxidation, if any. In case of semi-oxidized samples, it also gives information on the extent of oxidation.

XPS has also improved, with the availability of purer monochromatic X-ray sources leading to more accurate analysis of elemental chemical bond structures. Its evolution has been correlated to progress in electronics - controls and progress in ultra-high vacuum (UHV) pumping technology. It is used extensively to characterize high end and expensive semiconductor materials for checking their impurity profile, for failure analysis in electronic process manufacturing and for process related issues. Subsequently, different inorganic compounds, different salts, oxides, their constituents, and impurities have been extensively studied using XPS analysis [3, 4, 5]. It has also been used to understand the chemical bonding pattern of different complex polymers and associated chemistry. However, such polymeric and organic materials often have a high vapour pressure, while XPS is an ultra-high vacuum-based technique. So, they were not quite compatible for a long time, until researchers successfully cooled these samples to liquid nitrogen temperatures. Inorganic samples with water of crystallization and with such vapour pressure and degassing problems could now also be analysed by XPS. Metals and alloys, in general, pose no problems in terms of degassing. But porous metals may at times degas for a while in vacuum. So, in theory, metals and alloys are quite fit candidates for analysis by XPS/ HR-XPS [3,4, 5]. However, often, different metals and alloys are, less expensive to prepare and hence economically are less fancy items for analysis by such high-end analytical techniques.

Better and more improved electron optics has over time, improved the detection limit of impurities and superior detector electronics have significantly enhanced signal to noise ratios, leading to development of X-Ray Photoelectron Spectroscopy (XPS) with a better resolution and sensitivity. Detailed data libraries have evolved on all possible elements and their compounds for use with XPS, to the extent that one can make a good guess on possible content and concentration of most unknown samples. Here we use the advantage of XPS for a comparison of similar oxidized iron-based alloy ribbons and establish its credibility as an independent analytical technique, understand their relative alloy composition, their chemistry and state of oxidization, and also understand its expected performance - in a situation where other non-destructive analytical techniques e.g. EDAX or XRF are not very definitive. XRF is not always sensitive inaccurately detecting lower atomic number elements like oxygen, carbon nitrogen or their chemical constituents, while EDAX often overstates the constituents at lower atomic masses. We shall try to explore setting up of protocols, if feasible, to compare alloys using XPS. Fifteen iron based non-commercial experimental i.e. research grade alloys for possible use as magnetic sensor materials and CRGO steel were considered for our analysis and inter-comparison of marginally different alloy chemistry using XPS so that the same methodology can be later implemented, if required, for other commercially exploited alloys keeping the role of future XPS analysis prospects in metals and alloys in mind [6].

2 Materials and Methods

The fifteen (15) thin iron-based alloys ribbons, marked M-1 to M-16 respectively are investigated for their compositions and constituents. Their preparation methodology is discussed in detail elsewhere [6]. The high temperature and ambient pressure of 1×10^{-2} mbar was not sufficient to stop oxidation of their surface. Slight changes and alterations in composition, and preparation parameters had been made from sample to sample. Their effects are analysed here in detail using XPS.

However much one might sputter to clean the surface, one would always be getting oxygen beneath. The primary constituent of the sample matrix here, Fe was mostly in amorphous or nano-crystalline form due to the nature of sample preparation methodology used [6].

An initial survey spectrum of these alloy samples was collected using a Kratos Axis Ultra instrument, having a charge neutralization system and magnetic immersion lens, at room temperature at a pass energy of 300 eV and a step width of 0.2 eV. Based on this data, X-ray photoelectron spectroscopy (XPS) analysis of these thin ribbon type alloy samples were then done using the same Kratos Axis Ultra instrument, at room temperature, but using a pass energy of 5 eV and a step width of 0.1 eV. We wished to see the performance of this type of instrument configuration under such experimental conditions. It had a double- crystal based monochromatic X-ray source. All samples were Argon ion sputtered for 100 seconds before data collection.

The argon sputter energy used was of 4KeV. The sputter-cleaning spot size is of a few mm diameter/ dimension. The overlapping (co-axial) X-ray spot size is also similar in size. Time of sputter-cleaning of 100 seconds of sputter is based on past experience for removal of sample contaminants in this instrument. It is a trade-off between removing contaminants as opposed to removing a whole lot of top surface matter itself. The analysis chamber vacuum was maintained at or better than 7×10^{-9} mbar. During analysis, the analysis chamber vacuum was about 3×10^{-8} mbar. We wished to test, if in reality, in this particular instrument with its magnetic immersion lens i.e. magnetic focusing lens placed just below the sample holder, the 5eV pass energy data is as good as obtained by 20eV pass energy data from other XPS instruments without the immersion lens. In this case, the instrument's calibration status and quality of data was checked by using spectra from copper and a pure Ag reference film (fixed to the body of the sample holder) using the same 5eV pass energy. No correction was required for these standard reference samples. On the other hand, for samples that are inherently strong insulators or polymers, a setting of higher value of pass energy would have been the norm [7].

3 Results and Discussion

Data analysis and detailed peak fitting related work was done using a licensed CasaXPS software. During the fitting process, in all cases, for all samples, efforts had been made to fit similar peaks with similar FWHM values using constrained fits for a better comparison and better understanding of the chemical bonding. Shirley background was taken for computation of relative composition profile of each sample and for general curve fitting. The principal constituents of each sample are presented in Table 1. Kratos RSF values applicable for Axis Ultra had been used in the calculation. The major elemental constituents in general were C, O, Fe, Co, Si, Cu, Al, Ni, Mn, Cr, Nb and Zn were at times seen as minor impurities. However, their relative quantities varied a lot from sample to sample. The components of the individual peaks were considered for best physically possible fit, keeping in mind the literature report for similar fit related FWHM values where ever available. The fitted profiles were considered to have a 80% Gaussian and a 20 % Lorentzian mixed character. XPS related peak assignments were based on different established standard literature, references and our own assessment of the situation for each possible bonding during data analysis using CasaXPS software. The analysed data, including fitted data, raw data and background were finally plotted using Origin 7.5 software. Each figure of each graph from Fig. 1 to Fig. 12 has several components, as per data from each sample. In many of these samples, the inner shell XPS peaks were not observed due to their almost amorphous or nano-crystalline nature. We then have each of the individual fitted peak components, presented by a dotted line, while the Shirley background is shown as a dashed line. Based on all these individual components, we get the overall fitted data, presented in black continuous smooth curve format for all figures Fig.1 to Fig.12. It superposes on the experimentally obtained data. If in doubt about existence of a peak, a derivative of the spectra in that region in question was used to check for an inflection point.

Calibration of XPS data was done using the C1s peak from the samples. As a convention,it was

Table 1 — Relative composition variation of constituents in atomic % as calculated from XPS survey spectra

Sample Name	C %	O %	Fe %	Co %	Si %	Zn %	Cu %	Al %	Ni %	Mn %	Cr %	Nb %
M-1	10.2	46.1	20	5.9	5.5	0	0.3	1	11	0	0	0
M-2	0.9	27.4	50.5	5.2	2.1	0.2	0.7	0	12.3	0.1	0.5	0
M-3	4	29.4	51.6	6	1.9	0.3	1	0	4	1	0.6	0
M-4	1.2	36.4	39.8	6	1	0	0.3	0	14	2	0	0
M-5	6.3	42.5	22.5	9.2	3.4	0	2	0	6.7	7.2	0.2	0
M-6	4.4	21.2	12.4	2.8	0.8	1.9	0	13.2	22.7	18.6	1.8	0
M-7	10.8	21.8	41.7	5.3	1.7	0	1	1	14.1	0.1	2.5	0
M-8	0.1	36.4	38.9	5.5	1.4	0.4	0.7	0.2	14.8	0.1	1.2	0.5
M-9	17.4	20.5	36.8	5	1.6	0.2	0.7	2.7	11.6	0	3.2	0.2
M-10	1.1	31	45.2	5.3	2.3	0	0.8	0.6	12.6	0.2	1	0
M-11	4.5	24.8	44.5	5.8	1.8	0	0.6	4.5	12.5	0	1	0
M-12	20	42	17.2	5.1	1.8	0.1	0.2	1.4	11.8	0.3	0	0
M-13	0.4	37.6	37.4	6.4	1.2	0	1.2	0	15.3	0.6	0	0
M-14	4.2	26.9	42.3	17.9	1.7	0.2	1.8	0	2.7	0.1	2.3	0
M-15	7.4	31.6	37.8	5.9	1.3	0	0.9	0.1	14	0	1	0

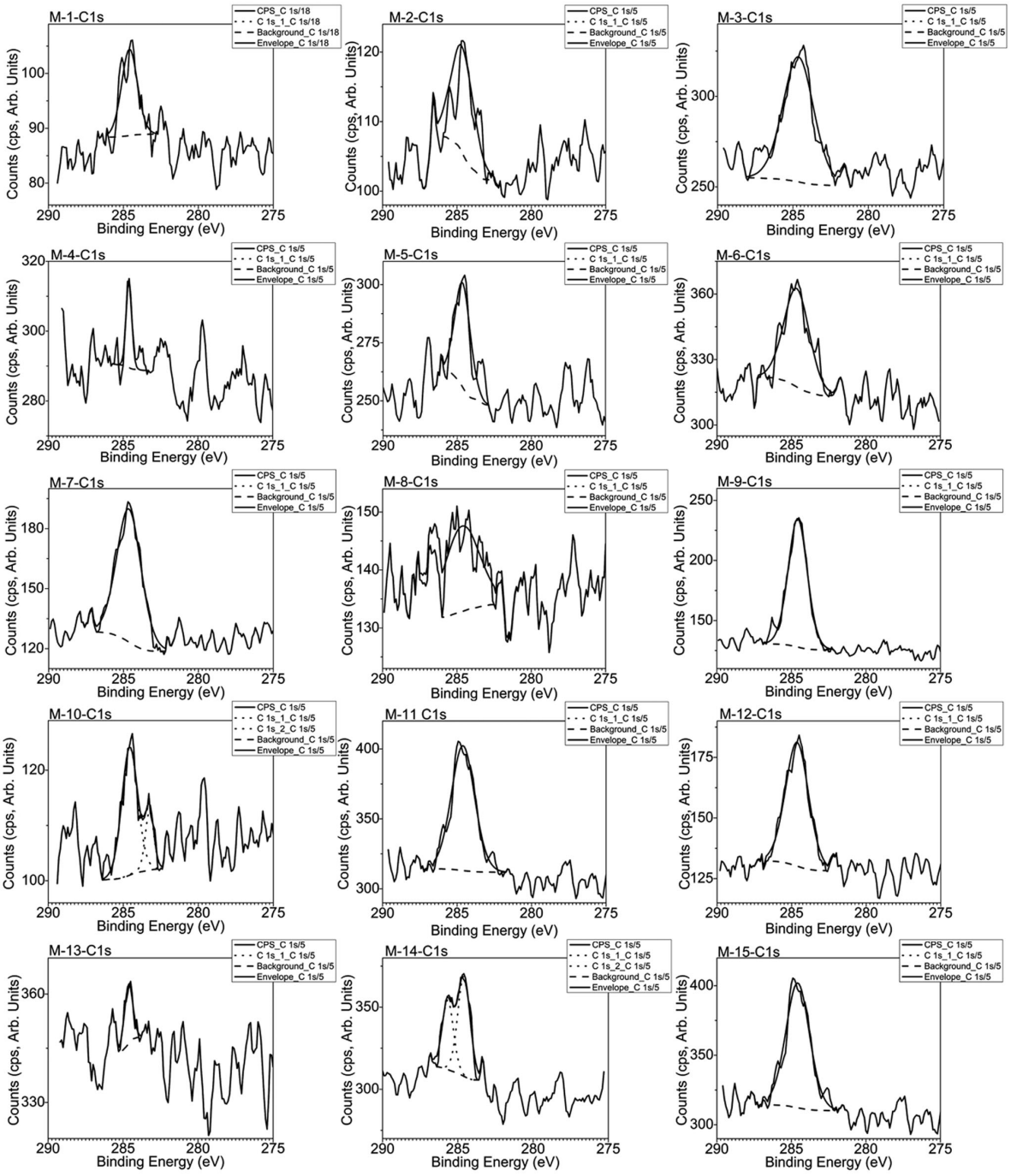

Fig. 1 — Shows the C1s binding energy (BE) spectra for these oxidized alloy ribbon samples.

standardized at 284.6eV for the graphitic carbon peaks [8]. The C1s peak for all the 15 samples are plotted in Fig.1.In some of the samples', the signal from the C1s is poor. So chances of errors in calibration of peak centre can increase in such cases.

The nominal elemental composition of different samples M-1 to M-15 are shown in Table 1. The details on representative elemental composition peaks are discussed separately in subsequent paragraphs. In lower concentrations, it was seen that such survey spectrum-based quantification is at times unable to accurately match a few lower concentration impurity elements, as compared to the detailed spectra. possibly due to nano crystalline /amorphous nature of these samples – related signal quality, subsequent pass energy and related signal quality. Fe is the primary constituent in all cases. These

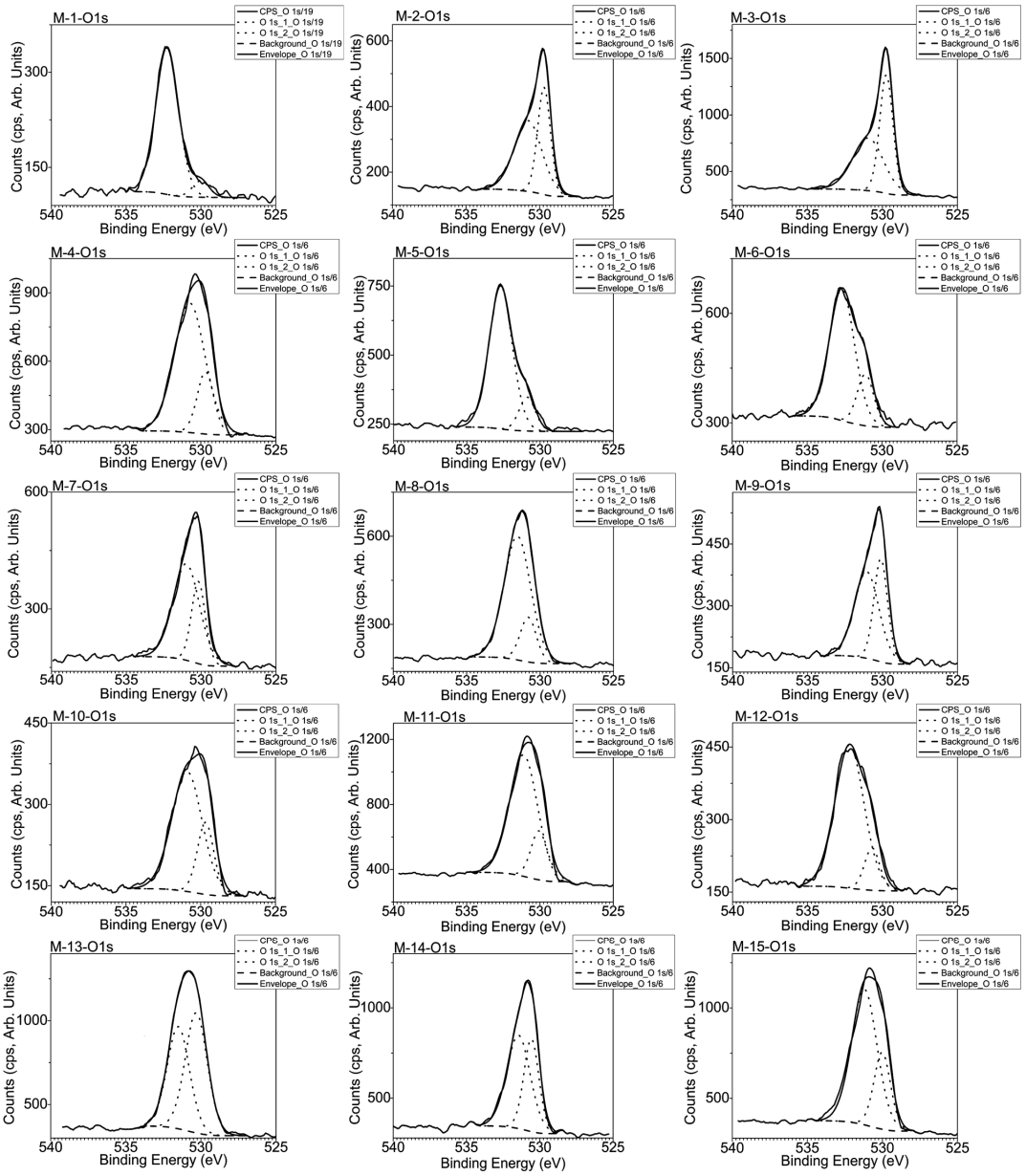

Fig. 2 — Shows the O1s binding energy (BE) spectra for these alloy ribbon samples.

are not electronic purity grade materials. Due to alloying – preparation methodology used, several intended and unintended impurities were seen. One has to thus keep the extent of purity in mind during analysis of such metal alloys. In this case, due to intended usage and methodology of preparation – including the vacuum levels used, oxygen is grossly present in all samples. In case of iron alloy based samples, there is often the desire to reduce the final carbon content. So some of the samples have much less carbon.

Strong oxygen O1s peaks were also present in all the 15 samples at around 530 eV with two constituent peak components [Fig. 2]. So, using O1s peak positions, all samples calibration could be checked. Jim Castle had also reported on such secondary calibration / checking of data using oxygen, under certain situations, for metals and alloys [9].

In all the 15 samples studied, O1s had two peak components (in dotted lines), though their relative profiles, intensities and peak areas varied from sample to sample [Fig. 2]. Due to the preparation methodology used, oxygen is omnipresent in all samples, as seen in Table 1 - the expected sample usage requirements were also such. The first peak was centred at around 530 eV,

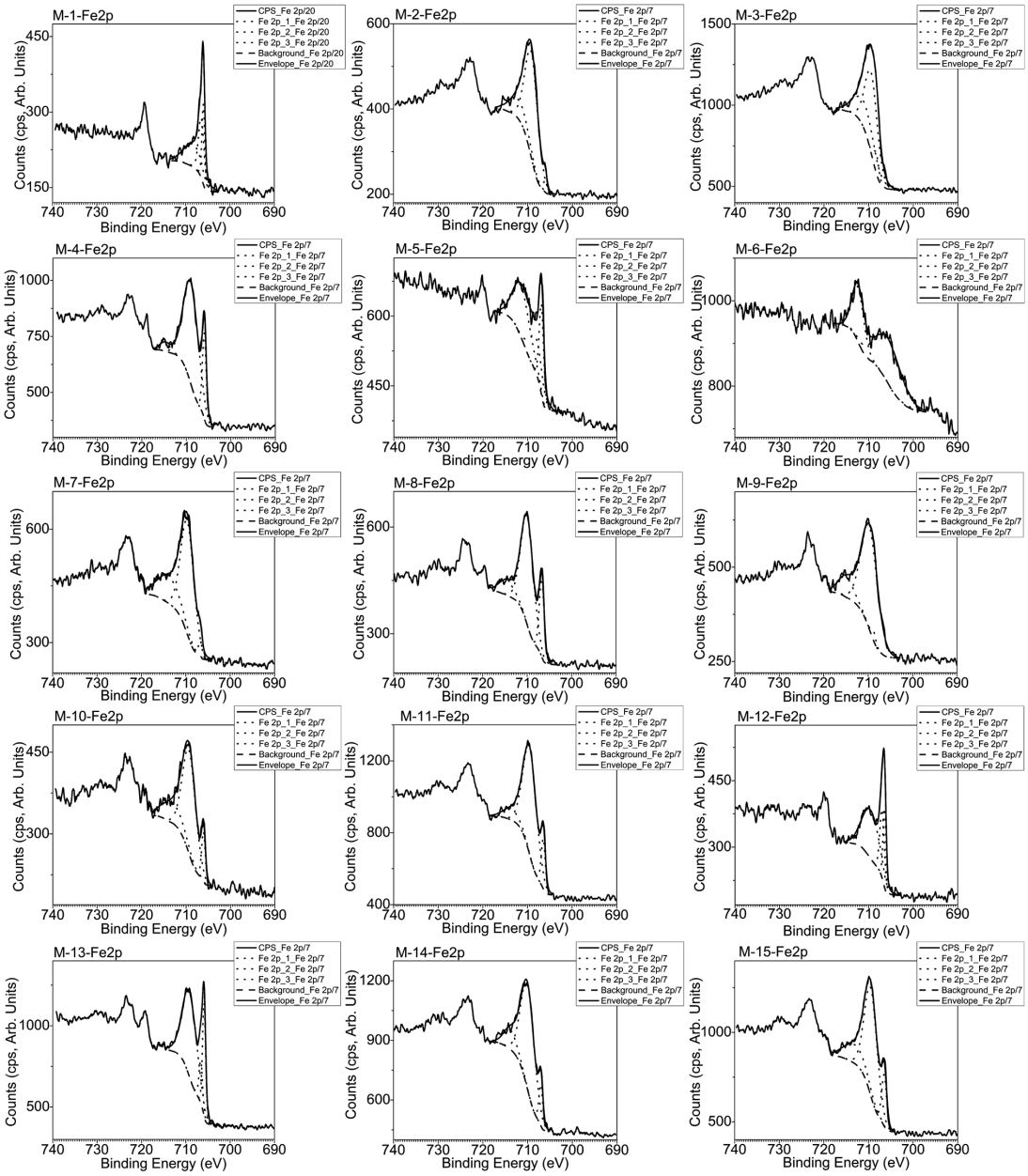

Fig. 3 — Shows the Fe2p binding energy (BE) spectra for these ribbon type iron alloy samples.

with a best fitted FWHM value of 1.2 eV for all samples, and could be ascribed to formation of Fe_2O_3, due to residual oxygen at the temperature of sample preparation [10]. The second peak was at 531 eV, with a FWHM of 1.8-2 eV and could be ascribed to adsorbed residual OH / other oxide bonds from one of the metal constituents as starting elements [11, 12]. Even though the starting elemental constituents of these Fe alloy samples were similar, due to slight variation in the processing parameters from sample to sample and differences in relative chemical reactivities of different constituents, there has been a competition for dominance between these two effects. So, the relative areas of these two peaks also varied from sample to sample. Such phenomena are also observed in other oxide compounds [12]. The methodology of these samples' preparation and processing procedure due to ambient oxygen at the temperature of preparation was thus understood, including pros and cons for the repeatability in sample preparation.

The XPS peaks for $Fe2p_{3/2}$at around 710 eV are shown in Fig. 3. Each of them are unique in their peak

profile / shape. Each had 3 best fitted components using constrained fits - at times each of them was very much distinguishable, and at times they were not so obvious until a detailed peak fit was done. The first fitted peak component, often explicitly visible, is at 706 eV is generally quite sharp in features with a FWHM of 1.2 eV – it may be attributed to elemental pure Iron which is partially present as a major constituent of the alloy matrix [8]. The second fitted component is at around 709 eV, and corresponds to the omnipresent Fe_2O_3, with a FWHM of 3.4eV, due to the preparation methodology used [10, 13]. The third peak is at 713 eV, and is quite broad with an FWHM of 5 eV and we feel that it possibly corresponds to more complex iron-based complexes present due to the alloying effects. Since this is rather a summarized - combined effect due to other constituents present in the alloy, its position also varied a bit, depending on such constituents and their relative content, including the relative extent of oxygen coverage and its variation from sample to sample, as may be seen from Table-1. In special cases, the peak at 709 eV had widened to an FWHM of 4 eV or more and remaining area shifts to 714eV with a relatively reduced FWHM. In other events different than the majority seen here, especially where higher amount of elemental Fe was present, the middle peak became sharper and shifted to 706.5 eV or so with a much-reduced FWHM. Constrained fitting was attempted in each case to get to this conclusion. Small variation in binding energy between sample to sample as seen here for such peak components is possibly due to the relative proportion of other metal alloy constituents / impurities - their relative encapsulation, considering relative proportion of iron oxide in vicinity. Such observations also have been reported earlier by Campbell et.al for metal alloys and their admixtures [14]. Among all these oxidized alloy samples, inner shell binding energy (BE) peaks were less obvious due to their amorphous / nano-crystalline nature.

All samples studied had some reasonably common impurities' present in most of them, other than carbon, oxygen and iron (Table 1), in smaller quantities. As they were not the primary major constituents like Fe, and its amorphous / nano-crystalline nature as host matrix, their XPS signals were less intense. As an example, these were broad $Co2p_{3/2}$peaks shown in [Fig. 4]. It had two broad components, one at 782 eV with an FWHM of about 5 eV and the other at 787 eV, with a FWHM of about 8 eV respectively. However, in some samples, the component at 782 eV had shifted to 778 eV and were unusually sharp with a FWHM of about 1.1 eV, while adjacent peak shifted to 779 eV, with a FWHM of about 1-2 eV. Such sharp and shifted peaks w.r.t. others may be due to elemental, un-reacted Co within the Fe matrix in these samples. The $Co2p_{1/2}$peak was most of the time in the noise level or too small. Due to the broad nature of both the peak components for $Co2p_{3/2}$most of the time, it may be said that the peak at around 787 eV is due to oxide formation, while the adjacent peak can be considered to be due to even more complex ferrites that got formed most of the time for most of these samples also called ferrites within the iron matrix [15, 16, 17]. This suggests that with even slight change in processing conditions or constituents, the chemical structure within the Fe matrix can change. Due to less impurity content, it is never the less, a noisy signal. So, such fits are at best only approximate. Some other authors' report these peaks at a bit higher binding energies and they assigned it as a satellite peak [18].

Silicon was also one of the detectable impurities in these Fe based alloys and showed relatively perceptible $Si2p_{3/2}$peaks [Fig. 5]. It was a minor impurity. The observed peaks were broadly in two positions, at around 102 eV and 92 eV respectively. The peak at around 102 eV had a FWHM value of 2 eV. Generally, Si2p peaks in the range of 101 eV are attributed to silicon carbides[19], while any peak at around 103 eV is associated to SiO_2 [8, 20, 21, 17]e.g., as in sample M-5. Carbides can come from the residual carbon in the samples, while oxygen can come from the preparation methodology used. Some samples showed a rare small peak at 98 eV, possibly from unreacted elemental Si. The peak at 92 eV was an enigma [8]. It may be seen that Zn3p has a peak at around 92eV [8, 22]. This peak is however, not marked separately in the graph as Zn3p. We may attribute this hump to traces of zinc oxide or more probably, zinc-based ferrite impurities present in the alloy, possibly coming from impurities at the sample preparation stage itself. Incidentally XRF results had also detected presence of Zn in many of these sample[6].

$Cu2p_{3/2}$XPS peaks as impurity constituents were seen in some of these samples (Table-1). Representative data is shown in Fig. 6 [23]. At times, the peak could be separated into two components, a stronger one at around 932.4 eV and smaller shoulder at 933.5 eV. The stronger peak had a FWHM of 1 eV while most often, the smaller shoulder had a FWHM of about 1.7 eV or so. In some of them, this FWHM was broader.

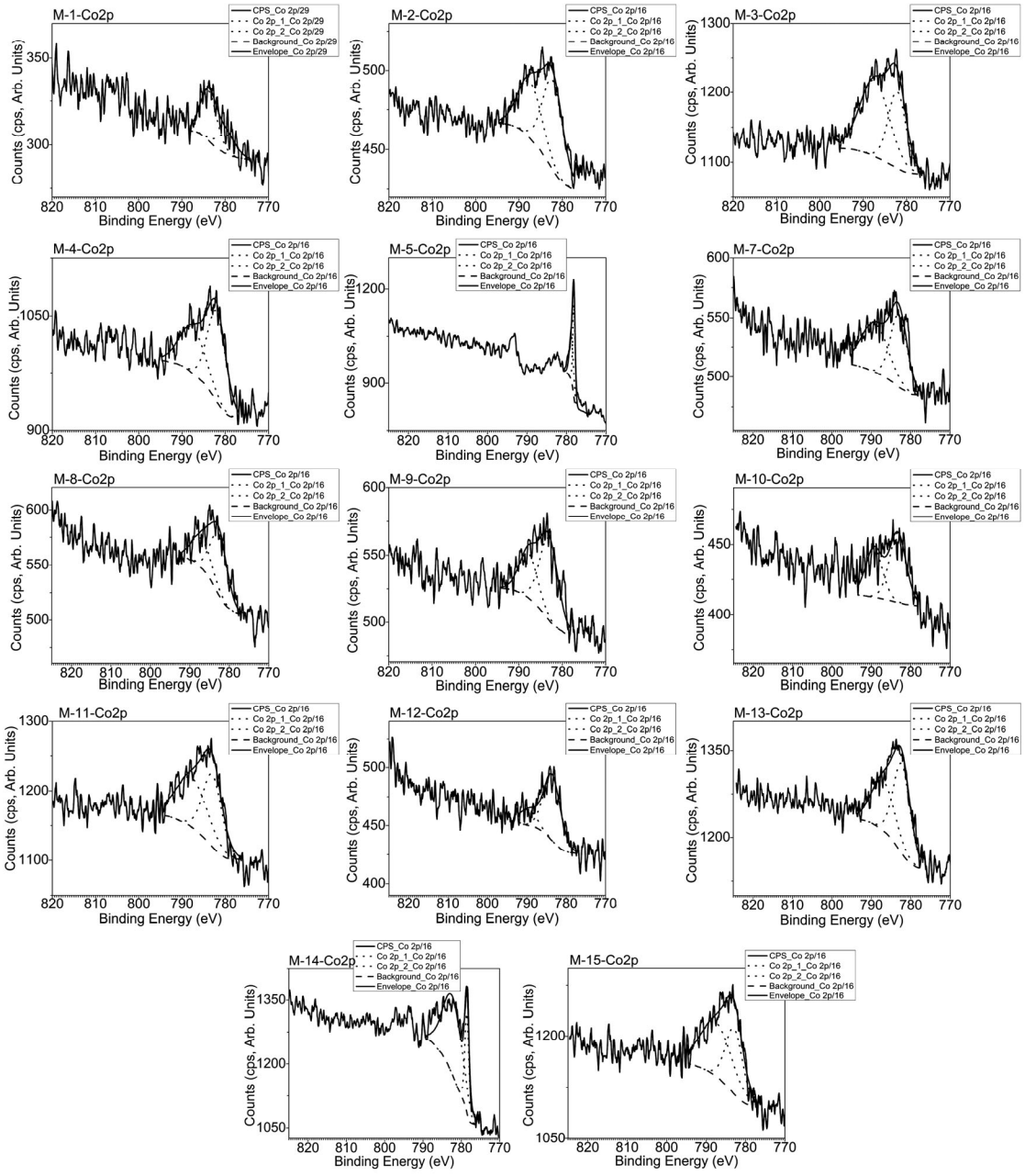

Fig. 4 — Shows the Co2p binding energy (BE) spectra for Co impurity seen in all the alloy ribbon samples.

The stronger / sharper peak with a small FWHM, possibly corresponds to elemental Cu as an impurity– it was the original intent and it had partially remained in unreacted condition and the shoulder is,in our opinion, possibly an oxide or ferrite component [8, 23, 24]. In case the Cu concentration and related signals were strong enough, the related $Cu2p_{1/2}$peaks were also visible at 952 eV.

Relatively stronger $Al2p_{3/2}$impurity peaks were observed only in some of these samples, e.g. in M-5 and M-6. In others they were relatively less [Fig. 7]. Here, two components could be separated out, one at 66 eV with an FWHM of 1.2 eV and the other at 67.5 eV, with an FWHM of 2.7eV respectively [17, 25, 26]. Aluminium is known to be quite easily reactive. So, the component at 67.5 eV is possibly due to complex oxides / ferrite formation while the one at 66 eV or so may be from elemental aluminium.

Presence of nickel Ni2p peaks as a “minor impurity”were detected in some of these samples

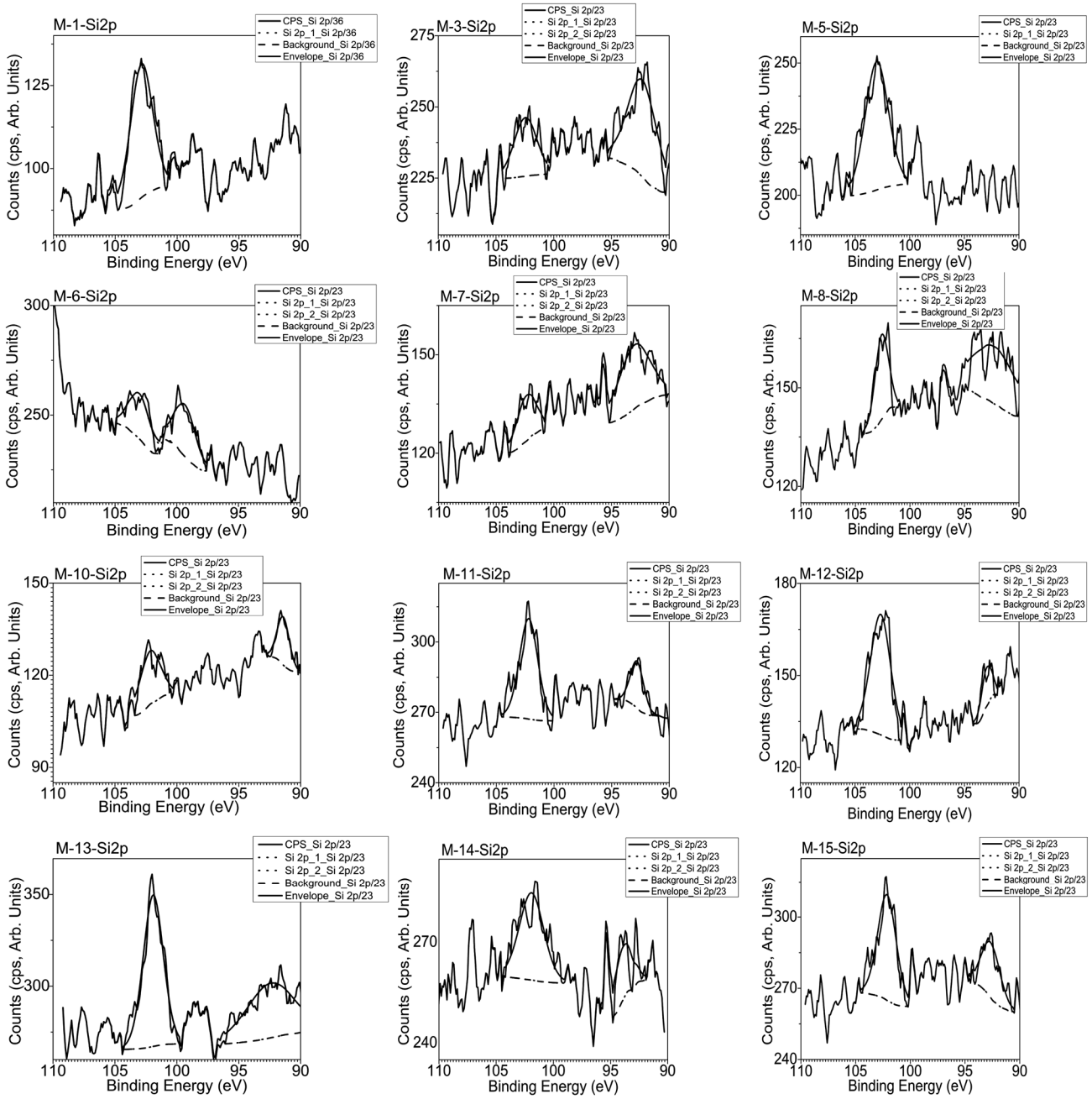

Fig. 5 — Shows the Si2p binding energy (BE) spectra. Si was seen to be an impurity constituent inmost of these alloy ribbon samples. However, Zn2p related peaks are also visible at times.

[Fig. 9]. As their concentration was often in lower limits, their peaks in such cases were also quite small. $Ni2p_{1/2}$ had merged into the background. They were broad, with two hump components at 845 eV and 851 eV, with FWHM values of around 5 eV for both humps . These are possibly related to elemental and different silicides formation when the peak component is closer to 853 eV or to metal oxide formation[8,27,28]. Only M-5 and M-6 showed a different sharp $Ni2p_{3/2}$peaks, with the peak centre at around 852.8 eV, with a FWHM of 1.1 eV or so, corresponding to unreacted elemental nickel along with a separately discernible $Ni2p_{1/2}$peak [28]. A separate smaller shoulder at 854.1 eV with a FWHM of 1.5eV was also seen in this case, attributable to partial nickel silicide / oxide formation.

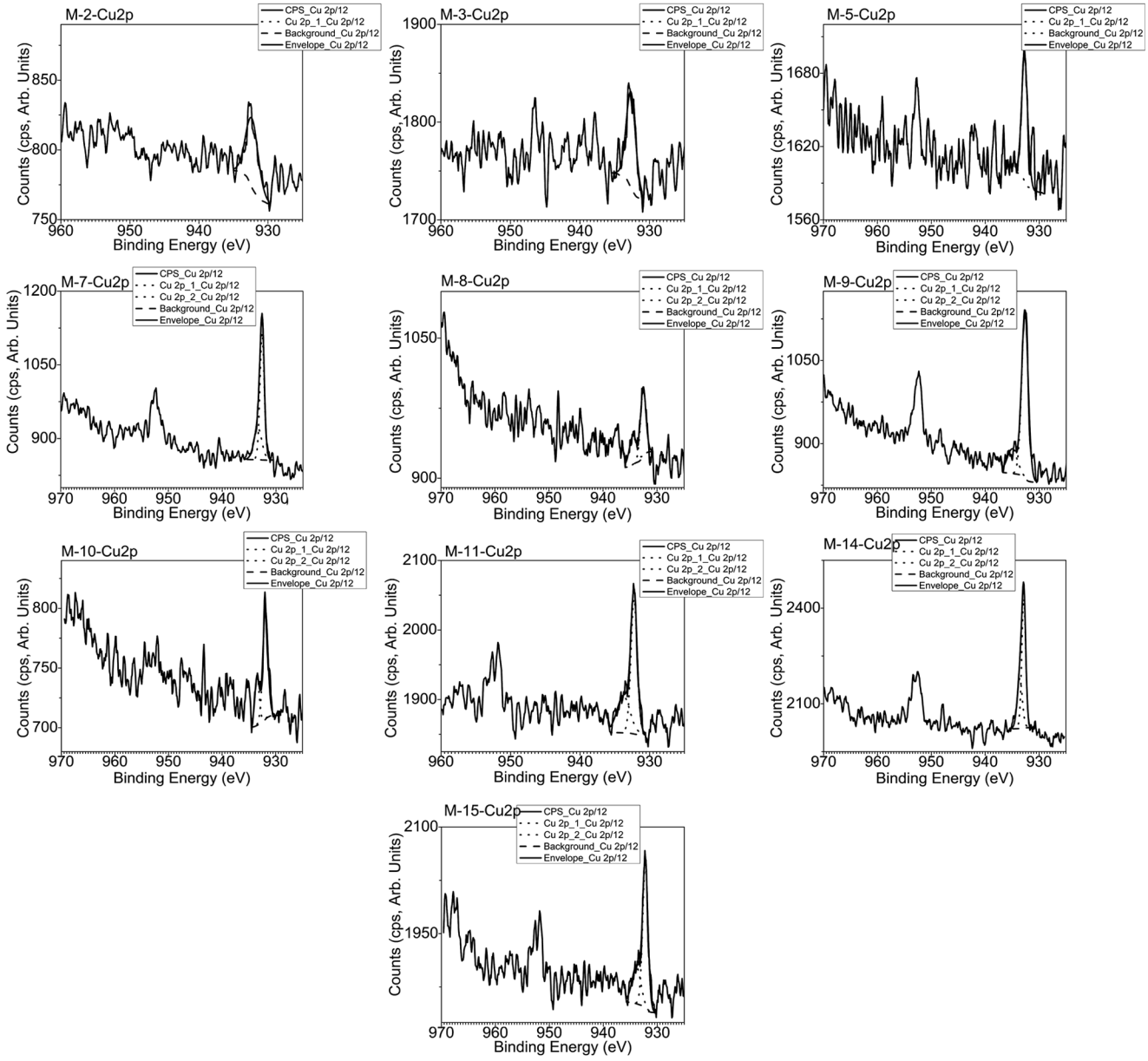

Fig. 6 — Representative Cu2p binding energy (BE) spectra for these oxidized alloy ribbon nano-crystalline samples.

Among these samples, only a few showed relatively stronger Mn impurity $Mn2p_{3/2}$XPS peaks, while most others showed only detectable amounts [Fig.9]. These had two broad components at 640.8 eV and 643.5 eV, with FWHM values of 2.3 eV and 2.8 eV or so respectively. A peak, if at around 639 eV can be assigned to elemental Mn [8, 29, 30]. The broadness may be due to oxide formation, like in other metal ions seen here. The shoulder at 643.5 eV may correspond to rare earth Eu Auger lines [8].

Cr is a very minor impurity in some of these alloys where they could be detected – e.g.$Cr2p_{3/2}$peak for sample M-6 is shown here [Fig. 10]. There were two broad components with peak centres at 574.5 eV and at 577 eV with FWHM of 2 eV and 2.7 eV respectively. The peak at 577 eV is attributable to oxide / ferritic oxide formation [30, 33, 34], while the lower BE peak at around 574.5 eV is possibly too shifted for any elemental $Cr2p_{3/2}$peak. Zn has Auger lines at around 573 eV [8]. So, traces of Zn in some samples are suggested.

Nb relatedNb3d impurity peaks were seen in three samples [Fig. 11], M-8, M-9, M-14 respectively in the region of 208eV or so [35]. In sample M-9, the relative

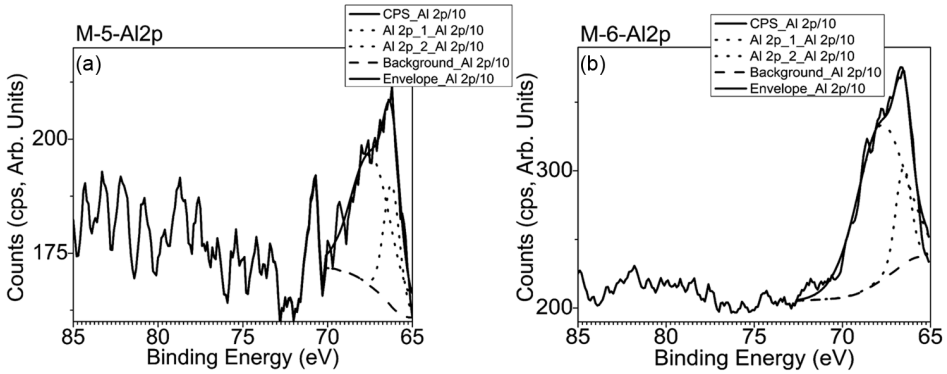

Fig. 7. — Representative Al2p peaks in these oxidized alloy ribbon type nanocrystalline samples.

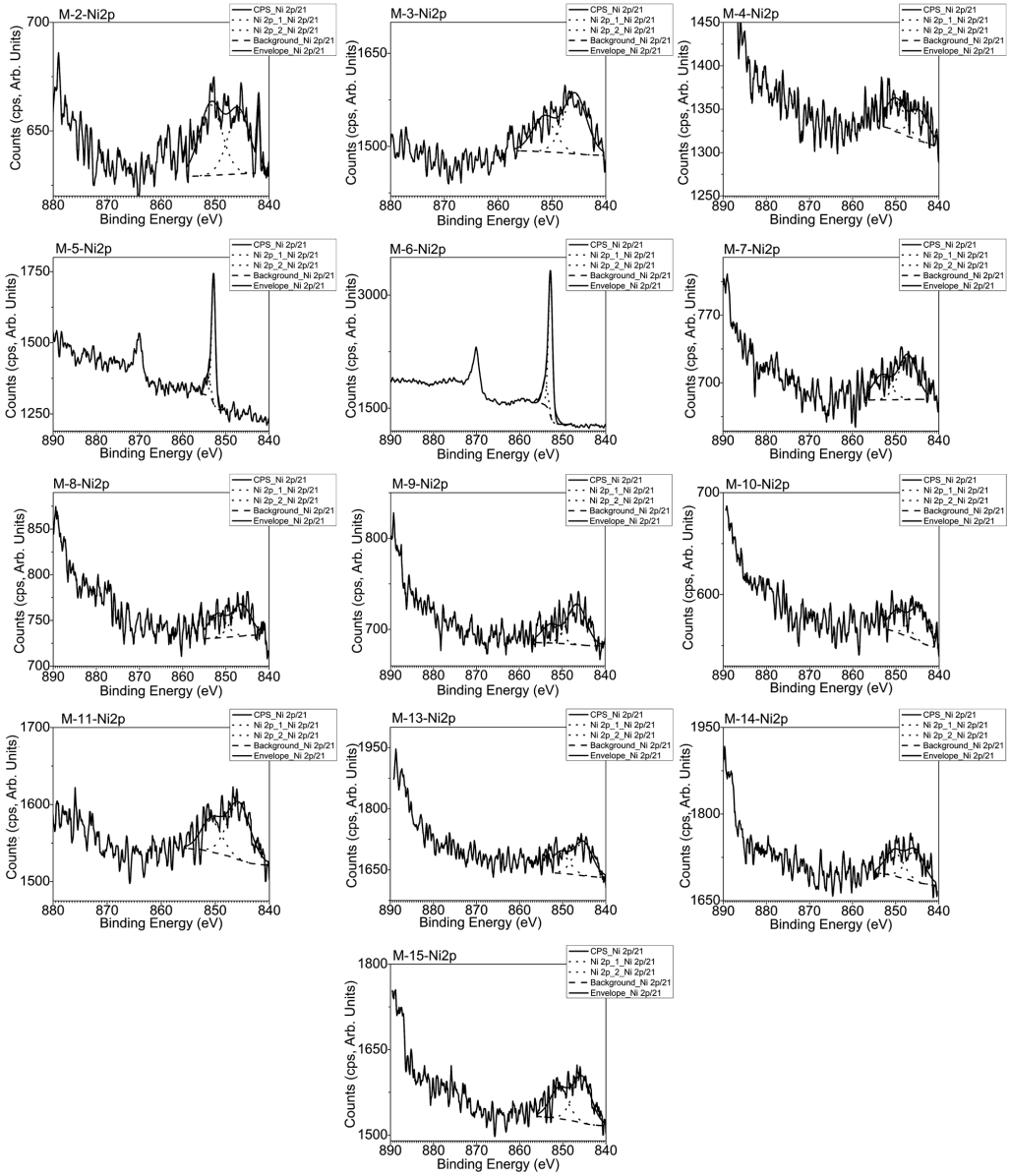

Fig. 8 — Representative Ni impurity as Ni2p binding energy (BE) spectra in these oxidized alloy ribbon nano crystalline samples.

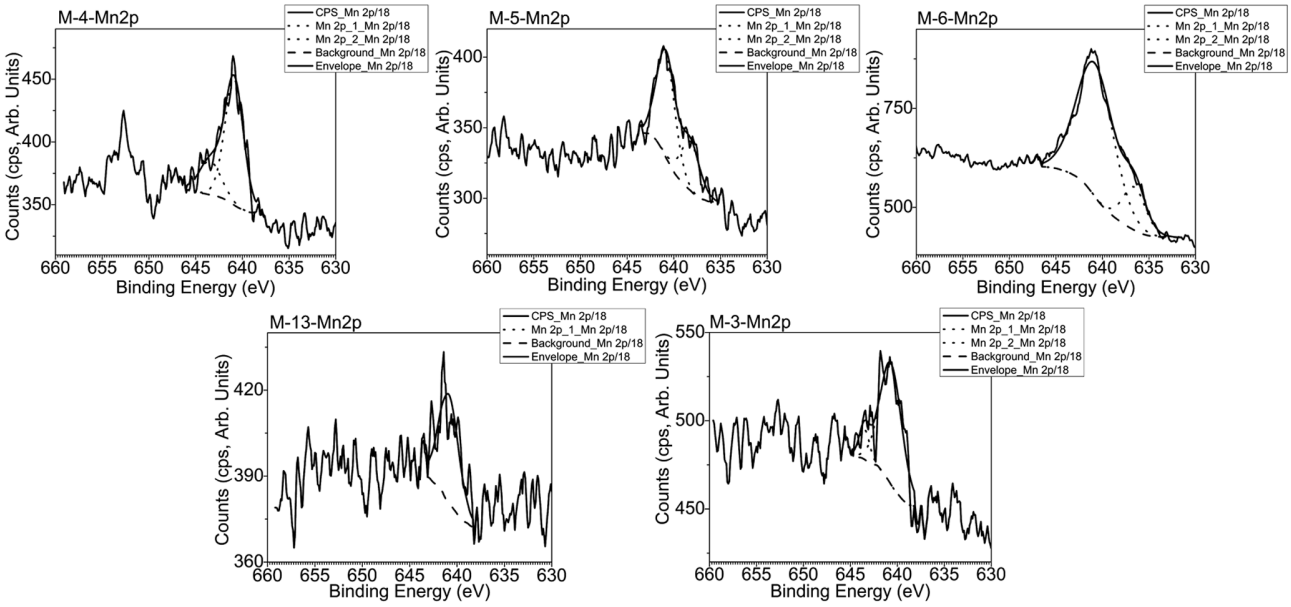

Fig. 9 — Relatively stronger representative Mn2p peaks in these ribbon type alloy nano-crystalline samp

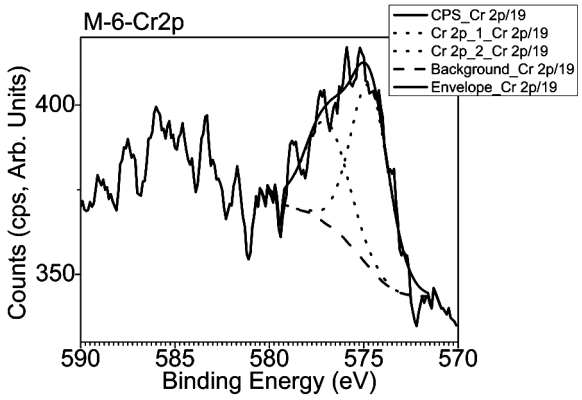

Fig. 10 — Representative Cr2p peak in such ribbon type alloy nano-crystalline samples.

Nb content was just detectable but closer to the noise level. The first BE peak position of 207 eV with FWHM of 1.5eV is correlatible only to Nb based oxide formation as peaks for elemental Nb are only at 202 eV [8, 35]. The second peak at a higher BE of 210 eV with FWHM of1.5 eV is possibly correlatible to Nb based ferrites.

Some of these samples also showed traces of phosphorous P2p peaks as trace impurities, with a peak at 128 eV or so with a FWHM of 1.6 eV [Fig. 12]. It is possibly in some complex ferrite form – but detectable just above the background noise level.

We have thus analysed 15 non-commercial, research grade oxidized iron alloy-based samples for possible use as magnetic sensor or as CRGO steel using XPS. The analysis composition data is summarized in Table-1, while the elemental peak and related fitting data is summarized in Table-2. They have similar but distinct constituent percentages. There are variations and differences in their crystalline features as well, that further segregate them from each other [6]. Their performance properties are thus expected to vary a lot.

Traditionally, metallurgists have not preferred routine XPS analysis of their alloys or related interpretations, while in most materials related to the electronics, chemicals and polymer industry, samples are routinely analysed in detail by XPS. In that context, we analyse what can we infer from such a detailed XPS analysis:

(a) We are able to compare relative compositions and chemical state in different metal alloys, irrespective of whether they are amorphous or nano-crystalline or crystalline.

(b) Constituent elements present in a particular alloy are better identified by XPS as compared to other analytical techniques, other elements can be detected non-destructively where EDAX or XRF had failed for that alloy [6]. Here, oxygen content in the sample is quite natural, as at the vacuum used, residual air content and moderate preparation temperatures ensures its incorporation into the matrix.

(c) In case of XRF or EDAX techniques, lower atomic number elements like carbon, oxygen,

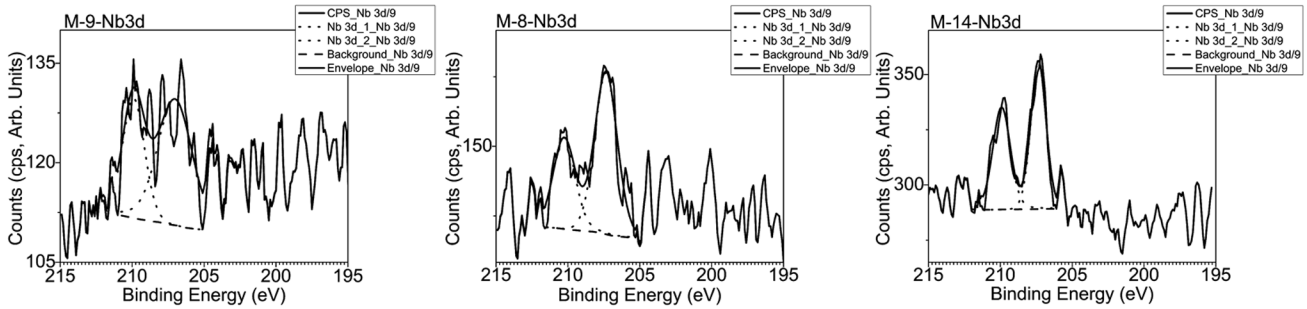

Fig. 11 — Three samples had relatively stronger Nb3d minor impurity peaks.

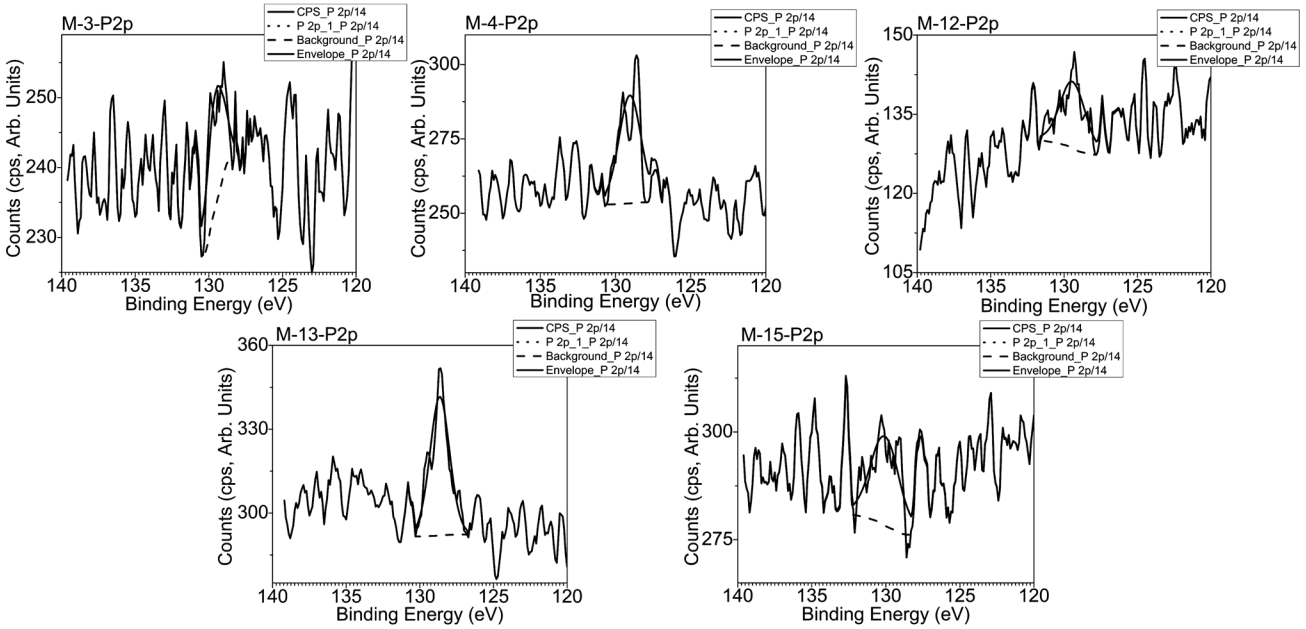

Fig. 12 — Some samples also showed phosphorous P2p related minor impurity peaks.

nitrogen, and some other elements like Niobium etc. are not always accurately detected in these alloys – rather they are often over quantified or totally undetected at times. In contrast, XPS is able to adequately inter-compare constituent percentages in such elements. In some cases, the XRF/ EDAX numbers obtained are so high that the whole quantification may seem unscientific for Fe based alloys. Essentiality of XPS based analysis is thus evident.

(d) XPS is not a destructive technique; so, the samples analysed were not unduly degraded after such analysis.

(e) Instrumental calibration of the XPS instrument used was ensured before data collection of our samples using this film samples of pure silver and copper. So, sanctity of XPS peak positions and related interpretations and analysis was ensured.

(f) XPS is not done for a point but over an area called spot size. So, data of a few mm diameter is collected - thus averaged and normalized information on elemental content is ensured.

(g) Ready inter- comparison of different alloy samples and composition analysis of each sample is possible using CasaXPS software, for such XPS analysis (Table-2).

(h) There is no matrix effort in such XPS analysis, unlike other UHV techniques, like say TOF-SIMS / SIMS.

(i) Different chemical state of constituents were immediately obtained and could be compared on a sample-to-sample basis. So, effects of preparation process differences like annealing or heat treatments e.g. time, temperature, vacuum and their effects in terms of carbon and oxygen content variation etc. can be immediately understood using XPS.

Table 2 — This table summarizes data from elements seen in each sample, their BE (eV) peak positions, possible peak constituents and their FWHM (eV) values.

Element	Constituent	BE (eV)	FWHM (eV)
C1s	Graphitic	284.6	2
Fe2p3/2	Elemental	706	1.2
Fe2p3/2	Fe_2O_3	709	3.4
Fe2p3/2	ferrite	713	5
O1s	Fe_2O_3	530	1.2
O1s	OH / ferrite	531	2.1
Co2p3/2	elemental	778	1.1
Co2p3/2	Oxide	782	5
Co2p3/2	Ferrite	787	8
Si2p	Oxide	102	2
Zn3p	Oxide	92	2.2
Cu2p3/2	Elemental	932.6	1.1
Cu2p3/2	Oxide / ferritic	934	1.7
Al2p3/2	Elemental	66	1.2
Al2p3/2	Oxide /Ferrite	67.5	2.7
Ni2p3/2	Elemental	845	5
Ni2p3/2	Oxide	851	5
Ni2p3/2	Silicide	852.8	1
Mn2p3/2	Oxide	640.8	2.3
Mn2p3/2	ferritic	643.5	2.5
Mn2p3/2	elemental	636.5	2.9
Eu	Auger	636	1.9
Cr2p3/2	Oxide	574.7	2.4
Cr2p3/2	Ferritic	577	2.7
Zn	Auger	572.6	2.5
Nb3d	Oxide	207	1.5
Nb3d	Ferrite	210	1.5
P2p	Ferrite	128	1.6

(j) Metallurgists do not wish to believe in any deficiencies of their processes unless they are faced with such reliable composition data. XPS analysis detects extent of purity of starting elements during preparation process so that the source of unwanted impurities is easily identified.

(k) Effects of intended or unintended impurities on the alloying process are readily identified by XPS in terms of type of chemical bonds formed and such information is able to correlate other properties like hardness, ductility or brittleness expected and obtained and their possible causes- these are often associated with impurities and their bonding profiles, their relative content and changes during processing, along with associated changes in their micro-structure.

(l) Tensile strength, Young's modulus, melting point and such parameters that are routinely used to check quality of alloys have indirect correlation with such composition. So, benefits of a detailed XPS analysis for alloys are immense.

We have used a representative set of research grade iron-based alloys to convey our point, without any commercial harm to any existing product. Commercial alloys and their quality can thus be controlled much better if XPS analysis is done and data is intelligently used and interpreted in an unbiased way.

4 Conclusion

We have presented XPS data for a set of oxidized iron-based ribbon type alloy samples with slight variations in composition and differences on preparation conditions. Traces of carbon in peak calibration also suggests on the quality of the iron alloy preparation. Unless, high vacuum-based alloy preparation is done, oxidized alloys like these shall be expected. Oxygen related XPS peaks in Fe alloys also provide a lot of secondary information e.g., extent of success in controlling the oxidation of an alloy during the preparation stage or extent of completion of iron preparation during the metallurgical chemical extraction process. Constituent impurity related BE peak position and profiles are not necessarily identical and vary from sample to sample, even though these are similar iron-based alloys, - due to different extents of oxidization and silicate or carbide or such compound formation differences in samples. As these are not electronic grade materials, unexpected XPS peaks will be observed, and can be related to some impurities. In an alloy preparation, unless all starting elements are checked for their purity and impurity levels, and repetition in all preparation conditions are ensured, sample to sample and batch to batch differences can exist due to differences in secondary impurities and their concentration profile.

Acknowledgements

CSIR-HQ, New Delhi and Director, CSIR-NPL are thanked for the funding support through MLP-201332. Dr. Rajat Roy and Dr. M. Prem Kumar of CSIR-NML are thanked for the samples. INUP-IISc, Bangalore is thanked for providing the XPS facilities.

Data Availability Issue

Raw data from the experiments at our end are in principle available upon reasonable request and reasonable, sufficiently justifiable cause from the corresponding author.

Financial Interests

The author does't have any direct financial interest in large scale commercial steel making or alloy

making or sale or financial proceeds thereof as on date. We also have no conflict of interest with any local or overseas steel or commercial alloy maker. The authors do not have any business interest with any analytical instrument manufacturer either.

References

1 Karar N and Jain V in Aswal D K, Yadav S (Eds.), Alloys as Certified Reference Materials (CRMs) Handbook of Metrology and Applications, Springer Nature Singapore Pte Ltd. (2022)

2 Zhang S, Li L, and Kumar A, Materials Characterization Techniques, CRC Press, (2008)

3 Briggs D and Seah M P, Practical Surface Analysis: Auger and X–ray Photoelectron Spectroscopy,Wiley, (1990)

4 Baer D, Artyushkova K, Brundle C, Castle J, Engelhard M, Gaskell K, Grant J , Haasch R, Linford M, Powell C, Sherwood A S, and Smentkowski V, *J. Vacuum Science & Technol.* A 37 (2019) 031401

5 Greczynski G, and Hultman L, *Progress in Materials Science*, 107 (2020) 100591

6 Karar N and Jain V, *AIP Advances*, 13 (2023) 035008

7 Bacon S, Brierley M, Baker M, Watts J, *Surf Interface Anal.*51 (2019) 849

8 Chastain J, King Jr R C (Eds.), Handbook of X-ray Photoelectron Spectroscopy, Physical Electronics, Minnesota, USA, (1992).

9 Caste J, *J Vac Sci Technol* B, 25 (2007) 1.

10 Carraro G, Gasparotto A, Maccato C, Peeters D, and Barreca D, *Surf Sci Spectra,*21 (2014) 1

11 Carraro G, Barreca D, Gasparotto A, and Maccato C, *Surf Sci Spectra,*19 (2012) 1.

12 Yamazoe N, Teraoka Y, and Seiyama T, *Chemistry Lett,*10 (1981) 1767.

13 Grosvenor A P, Kobe B A, Biesinger M C and McIntyre N S, *Surf. Interface Anal.,*36 (2004) 1564.

14 Campbell R, Rodriguez J, and Goodman D W, *Physical Review:B*, 46 (1992) 7077

15 Diodati S and Gross S, *Surf Sci Spectra*, 20 (2013) 17

16 Haasch R and Abraham D, *Surf Sci Spectra*, 23 (2016) 118

17 Canon J, and Teplyakov A, *Surf Interface Anal.,*53 (2021) 475

18 Kocijan A, Milosev I, and Pihlar B, *J Mater Sci: Mater in Medicine*, 15 (2004) 643

19 Contarini S, Howlett S P, Rizzo C and Angelis B De, *Appl. Surf. science*, 51 (1991) 177.

20 Haasch R, Patscheider J, Hellgren N, Petrov I, and Greene J, *Surf Sci Spectra*, 19 (2012) 42.

21 Jensen D, Kanyal S, and Madaan N, *Surf Sci Spectra*, 20 (2013) 36.

22 Strohmeier B, *Surf Sci Spectra,*3 (1994) 128.

23 S. Diodati, A. Minelli, P Dolcet, and S. Gross, *Surf Sci Spectra,*22 (2015) 1.

24 Batista J, Pintar A, Mandrino D, Jenko M, and Martin V, *Appl Catalysis A: General,*206 (2001) 113.

25 Sherwood P, *Surf Sci Spectra,*5 (1998) 1.

26 Myhre K, Meyer H and Du M, *Surf Sci Spectra*, 23 (2016) 102.

27 Haasch R and Abraham D, *Surf Sci Spectra,*23 (2016) 118 .

28 Nesbitt H W, Legrand D, and Bancroft G M, *Phys Chem Minerals,*27 (2000) 357.

29 Diodati S and Gross S, *Surf Sci Spectra,*20 (2013) 17.

30 Biesinger M, Payne B, Grosvenor A, Lau L, Gerson A, and Smart R, *Appl Surf Science,*257 (2011) 2717.

31 Nelson A, Hildebrand N, and Major P, *Surf Sci Spectra,*9 (2002) 250.

32 Eighmy T, Kinner A, Shaw E, Eusden J, and Francis C, *Surf Sci Spectra,*6 (1999) 210.

33 Rossi A, Tulifero R and Elsener B, *Mater and Corrosion*, 52 (2001) 175.

34 Epling W, Hoflund G, and Minahan D, *Surf Sci Spectra,*4 (1996) 168.

35 Dacca A, Gemme G, Mattera L, and Parodi R, *Surf Sci Spectra*, 5 (1998) 332.